3

CHAPTER 3:   NUMERICAL MODELLING

3.1.   INTRODUCTION

This chapter deals with the processes that are involved in the numerical modelling of heat transfer and flow, discretisation of the computational domain, solving of the heat and mass transport governing equations and processing of the results. The commercial CFD software FLUENT [199] is used for the numerical analysis, which will be discussed in detail in the subsequent sections.

3.2.   MODELLING PROCEDURE

Recently time, the modelling of fluid flow and heat transfer problems have been made easy by the development of CFD codes structured around numerical algorithms. The numerical analysis consists of three stages, namely:

1. Pre-processing: This involves defining and developing the computational domain, geometry, mesh generation and discretisations, as well as the selection domain boundaries for the purposes of simulation.

2. Solver execution: This involves the integration and solving of the governing equations at various nodal points across the computational domain.

3. Post-processing: This involves the analysis of results and provision of visualisation tools such as grid displays, the generation of contour plots of various parameters of interest and particle tracking [200].

3.3.   GEOMETRY AND GRID GENERATION

Geometry and grid generation constitute a major part of the pre-processing stage in a CFD analysis. The process involves dividing the computational domain into a finite number of discretised control volumes on which the governing equations can be solved.

The Geometry and Mesh Building Intelligent Toolkit (GAMBIT) [201] is a commercial automated grid generator. With the help of a graphical user interface (GUI), it is used to construct finite volume models and create the geometry for generating meshes. The model and meshes are exported to FLUENT software for simulation and analysis. GAMBIT [201] and FLUENT 6.3 [199] can be automated by means of journal input files during optimisation process by setting up a computational model and mesh generation.

The governing non-linear partial differential equations used for the fluid flow and heat transfer analysis include the conservation of mass (continuity), conservation of momentum and conservation of energy - coupled through density-pressure relationship.

3.4.   CONSERVATION OF MASS

In an Eulerian reference frame, the equation of continuity in its most general form for fluids is given by [202]

$$\frac{D\rho}{Dt} + \rho \ \text{div} \ u = 0 \tag{3.1}$$

where ρ is the density of the fluid, t is the time and V is the velocity vector of the fluid. For incompressible flow (constant density), Equation 3.1 reduces to:

$$\rho \ \text{div} \ u = 0 \tag{3.2}$$

3.5. CONSERVATION OF MOMENTUM

The momentum conservation equation is formally derived from Newton's second law, which relates the applied force to the resulting acceleration of a particle with mass. For Newtonian viscous fluids, Navier and Stokes fundamentally derived the following equation using the indicial notation:

$$\rho \frac{DU}{Dt} = \rho \boldsymbol{g} - \nabla P + \frac{\partial}{\partial x_j}\left[\mu\left(\frac{\partial u_i}{\partial x_j} + \frac{\partial u_j}{\partial x_i}\right)\right] + \delta_{ij}\lambda \ \text{div} \ \text{U} \tag{3.3}$$

where $\boldsymbol{g}$ is the vector acceleration of gravity, P is the pressure, x is the spatial coordinate, μ is the coefficient of viscosity, u is the velocity component, δ_{ij} is the Kronecker delta function and λ is the vexing coefficient associated with volume expansion [202]. Using Stokes' hypothesis, $\lambda = -\frac{2}{3}\mu$.

For incompressible flow, the vexing coefficient λ and $\text{div} \ \text{U}$ (due to the continuity relationship) vanish, simplifying Equation 3.3 to:

36

$$\rho\left(\vec{u}\cdot\nabla\vec{u}\right) = -\nabla P + \mu\nabla^2\vec{u} \tag{3.4}$$

3.6. CONSERVATION OF ENERGY

The conservation equation is derived from the first law of thermodynamics, which states that an increase in energy is a result of work and heat added to the system. Neglecting radiative effects, the energy equation in its standard form can be written as:

$$\rho\frac{Dh}{Dt} = \frac{DP}{Dt} + \text{div}(k\,\nabla T) + \Phi \tag{3.5}$$

where h is the enthalpy of the fluid, k is its thermal conductivity, T is the temperature of the fluid and Φ represents the dissipation function expressed as:

$$\begin{aligned}
\Phi = \mu &\left[2\left(\frac{\partial u}{\partial x}\right)^2 + 2\left(\frac{\partial v}{\partial y}\right)^2 + 2\left(\frac{\partial w}{\partial z}\right)^2 + \left(\frac{\partial v}{\partial x} + \frac{\partial u}{\partial y}\right)^2 + \left(\frac{\partial w}{\partial y} + \frac{\partial v}{\partial z}\right)^2 + \left(\frac{\partial u}{\partial z} + \frac{\partial w}{\partial x}\right)^2 \right] \\
&+ \lambda\left(\frac{\partial u}{\partial x} + \frac{\partial v}{\partial y} + \frac{\partial w}{\partial z}\right)^2
\end{aligned} \tag{3.6}$$

For incompressible flow with constant thermal conductivity and low velocities, the viscous dissipation becomes negligible. Thus, Equation 3.5 can be simplified to:

$$\rho_f C_{Pf}\left(\vec{u}\cdot\nabla T\right) = k_f \nabla^2 T \tag{3.7}$$

while the energy equation for a solid with internal heat generation is given as:

$$k_s \nabla^2 T + q_s''' = 0 \tag{3.8}$$

where, k_f and k_s represent the thermal conductivity of the fluid and solid respectively. The simplified equations are in steady state.

3.7. BOUNDARY CONDITIONS

When a meshed geometry with grid is imported into FLUENT [199], boundary conditions for various surfaces and parameters need to be specified to run the simulations. The boundary conditions are guided by the types of engineering problems we want to solve.

3.8. NUMERICAL SOLUTION TECHNIQUE

This section deals with the numerical techniques implemented by using a three-dimensional coupled density-based commercial package FLUENT™ [199] in solving the mass, momentum and energy conserving equations that employs a finite volume method (FVM). The details of the method were explained by Patankar [203].

The computational domain is discretised into a finite number of discrete elements and control volumes. The combined convection and diffusion terms in the momentum and energy equations are integrated on each discrete element and control volume thereby constructing algebraic equations for the discrete dependent variables to be solved. The discretised equations are linearised and the resulting system of linear equations is solved to yield updated values of the dependent variables.

Furthermore, the governing equations which are non-linear and coupled are solved by segregating them from one another. Hence, several iteration processes of the solution loop must be performed [199] before a converged solution is obtained. A flow chart representing an overview of numerical steps of the iterative process is shown in Figure 3.1.
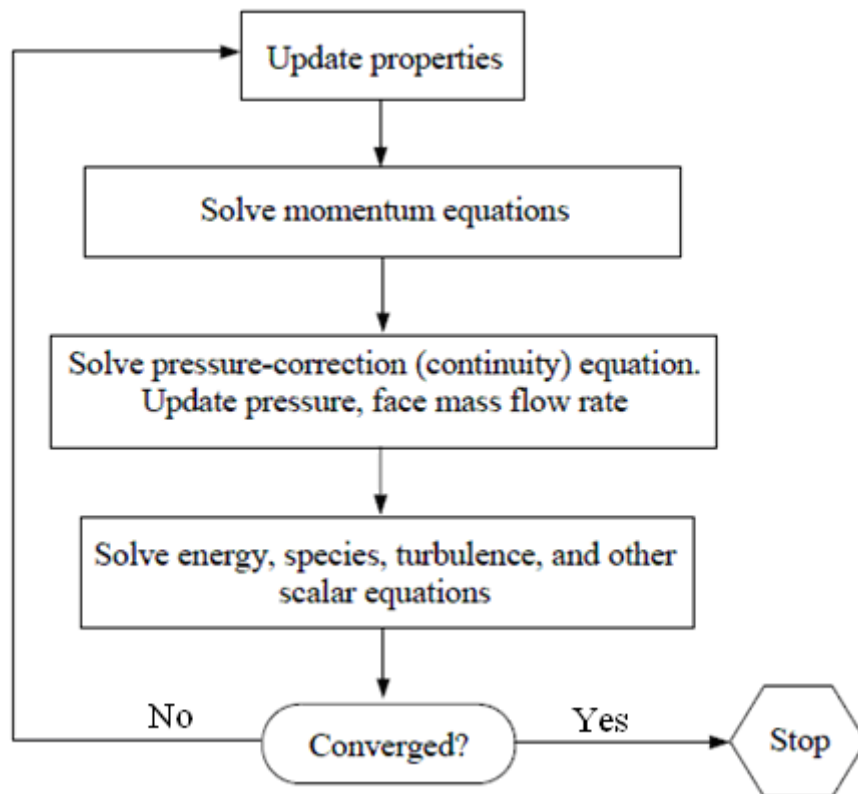

Figure 3. 1 : Overview of the segregated solution method [199]

3.9.   CONCLUSIONS

This chapter focused on the processes involved in solving fluid flow and heat transfer problems by using a three-dimensional coupled density-based commercial package FLUENT™. A set of non-linear partial differential equations governing the transport of mass and heat is discussed. The numerical scheme implemented in solving the flow and heat transfer is also examined.

CHAPTER 4:   NUMERICAL OPTIMISATION

4.1.   INTRODUCTION

This section examines the theory governing the mathematical optimisation algorithms used in this thesis, together with the numerical modelling technique described in Chapter 3. We also examine an overview of the optimisation technique, which is described in detail in the subsequent sections.

4.2.   NUMERICAL OPTIMISATION

The mathematical or numerical optimisation often known as non-linear programming is described as a systematic method to find the minimum or maximum of a specific function for a given set of constraints. This helps in finding the best design under certain design constraints by changing the appropriate design variables. It can also be defined as the solving of a problem or task in the best way that can be expressed mathematically or numerically. Optimisation models arise in almost every area of human endeavours. In economics, optimisation is the maximisation of profit, maximisation of efficiency and minimisation of loss or risk. In engineering, optimisation is the design of a building or machinery to minimise the weight or maximise strength in order to avoid failure. The history of mathematical optimisation date back to the 1940s when it was first used as steepest descent for solving very simple problems in cases where functions of many variables are considered[192].

4.3.   NON-LINEAR CONSTRAINED OPTIMISATION

In mathematical optimisation, an optimal solution is obtained by changing some parameters known as the design variables while the function to be optimised (minimised or maximised) is called the objective or cost function $f(\boldsymbol{x})$. The design variables are generally represented by a vector $\boldsymbol{x}*$. The optimisation problem becomes a constrained optimisation problem when some constraints in the form of inequalities $g_i(\boldsymbol{x})$ or equalities $h_j(\boldsymbol{x})$ are introduced into the process; else the problem is an unconstrained optimisation problem. The unconstrained optimisation problem is solved more easily, compared to a constrained optimisation problem. This is because the former is reduced to the search of finding the minimum or maximum values of the objective function $f(\boldsymbol{x})$. For the constrained optimisation problem, the optimisation becomes very complex. The constraints will have to be treated in a special way by introduction of a penalty function.

In general, the non-linear constrained optimisation problem can be expressed in mathematical form as

$$\min_{x} f(x); \left[x_1, \ldots x_2, \ldots x_i \ldots X_n, \right]^T, \; x_i \in \square^{\,n}, \tag{4.1}$$

subject to

$$g_j(x) \leq 0, j = 1, 2, \ldots p, \tag{4.2}$$

$$h_k(x) = 0, k = 1, 2, \ldots q, \tag{4.3}$$

where $f(x)$, $g_j(x)$, $h_k(x)$ are scalar functions of the vector x and they are defined as objective or merit functions, inequality constraint functions and equality constraint functions, respectively. The components of vector x are called design variables. The solution of the problem in Equations (4.1) to (4.3) is given as vector x^*:

$$x^* = \left[x_1^*, x_2^*, \ldots, x_n^*, \right]^T \tag{4.4.}$$

This gives the lowest value of the objective function $f(\boldsymbol{x})$ subject to specified inequality and equality constraints. In a situation where the objective function $f(\boldsymbol{x})$ is to be maximised, the minimisation algorithm is still applicable. However, the setting will be $f_{max}(\boldsymbol{x}) = -f(\boldsymbol{x})$. Figure 4.1 represents the transformation of the maximisation problem to a minimisation problem [192].
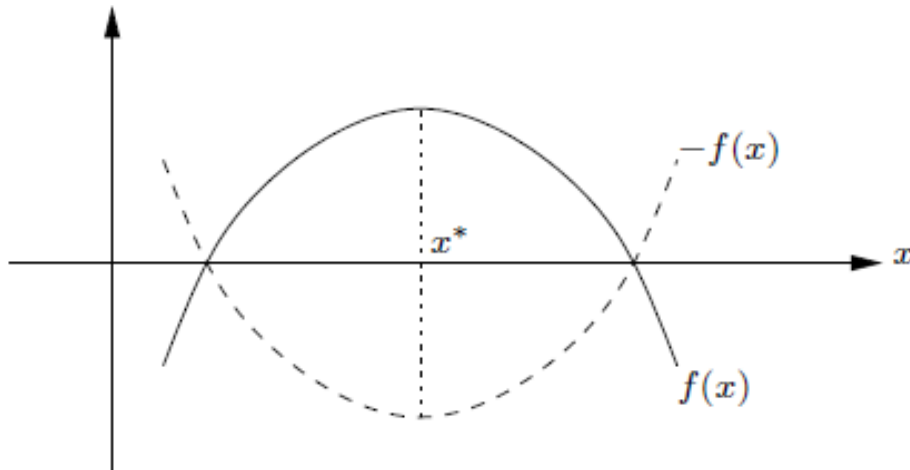
Figure 4. 1 : Graphical representation of a maximisation problem [192]

As stated in Chapter 2 different types of algorithms have been developed to solve the optimisation problem of Equations (4.1) to (4.3). These include the generic algorithm, multiplier methods, surrogate, annealing simulation, Powel algorithm and sequential quadratic programming [192]. Some mathematical algorithms are commercially available. However, new algorithms are being developed to solve the inhibiting complications experienced with the available methods. Only the optimisation algorithms used in this study are discussed next.

4.4.   OPTIMISATION ALGORITHMS

The Leapfrog Optimisation Program for Constrained Problems (LFOPC) and DYNAMIC-Q algorithms [204, 205] were used as optimisation processes in this study to optimise an approximation solution to the original problem. The LFOPC algorithm

is applied to the penalty function parameter in three phases, which increases the rate of searching for an optimal design solution in limited time. DYNAMIC-Q is a gradient-based algorithm and is good at handling optimisation problems with a large number of variables with minimal storage requirements of the computer RAM. Also, unlike genetic algorithm methods, the DYNAMIC-Q is not computationally expensive, as complex functions that are expensive to compute numerically are approximated using spherical quadratic approximate functions. Both LFOPC and DYNAMIC-Q algorithms are discussed in detail in the subsequent sections.

4.4.1. Leapfrog optimisation program for constrained problems (LFOPC)

Snyman's original LFOP [204, 205] was adapted to handle constrained problems of equality and inequality constraints by introducing a penalty function formulation of the original problem in three phases [206 - 208]. The penalty function formulated as

$$p(\boldsymbol{x}) = \gamma f(\boldsymbol{x}) + \sum_{i=1}^{m} \alpha_i g_i(\boldsymbol{x})^2 + \sum_{j=1}^{n} \beta_j h_j(\boldsymbol{x})^2 \tag{4.5}$$

where

$$\alpha_i = \begin{cases} 0 \text{ if } g_i(\boldsymbol{x}) \leq 0 \\ \rho_i \text{ if } g_i(\boldsymbol{x}) > 0 \end{cases} \tag{4.6}$$

To simplify the algorithm, the penalty parameters ρ_i and β_j take on the same positive value μ, that is $\rho_i = \beta_j = \mu$. As the value of μ increases, say $\mu = \infty$, the unconstrained minimum of $p(x)$ solves the constrained problem of Equations (4.1 – 4.3); hence the solution to the constrained problem becomes more accurate at a very high value of μ. The unconstrained optimisation problem on the other becomes ill-conditioned at a very high value of μ. Therefore, the penalty parameter should be increased gradually until it reaches the limit value of μ. The later is then kept constant until convergence is reached with minimum violation of the inequality constraints in the initial design steps [206]. The penalty function formulation of the constrained problem in Equation (4.2) occurs in three phases and will be next discussed as executed in the optimisation process.

4.4.1.1.   Penalty formulation: Phase 0

In this phase, for a given initial guess of the design variable $x_0 *$, the penalty parameter introduced is given a value of μ_0. The penalty function is subsequently minimised using the Leapfrog optimisation program (LFOP) and with $\gamma = 1$ resulting in an optimum design variable vector $x(\mu_o) *$ after convergence. The LFOP automatically scales the constraints to make sure that the violation of a constraint on the gradient of penalty function is approximately the same for all the constraints. At this optimal point, the active inequality constraints are checked and identified for

spatial violation. If no active inequality constraints are found (constraints that are violated), and no equality constraints either, this optimal point must certainly be the optimal minimum value of the optimisation problem and the algorithm is then completed.

4.4.1.2.   Penalty formulation: Phase 1

This phase is initialised by increasing the value of the penalty parameter μ when active inequality constraints are obtained from the solution of Phase 0. The penalty function parameter for objective constraints is again set to $\gamma = 1$. Also the approximate design point, $x(\mu_o)^*$ obtained from Phase 0 is used as the starting guess, after which the penalty parameter is minimised by LFOP. Following convergence, a more accurate solution of the original problem is found and active inequality constraints that may be different from that of phase 0 are again identified. If there are no active constraints, and the solution $x(\mu_1)^*$ becomes the optimal solution of the optimisation problem then the algorithm is terminated

4.4.1.3.   Penalty formulation: Phase 2

In this last phase, the penalty function parameter for objective constraint is again set to $\gamma = 0$. The optimal solution from phase 1 is used as the initial guess and the penalty parameter is then minimised by LFOP. The optimisation algorithm will search for an optimal solution of the optimisation problem, which corresponds to the intersection of

the active constraints. However, if the active constraints do not intersect, the optimisation algorithm will find the best likely solution, which is usually closer to the real solution with little active constraint violation.

4.4.2. DYNAMIC-Q optimisation algorithm

The DYNAMIC-Q optimisation algorithm was developed by Snyman *et al.* [204, 208 -210] at the University of Pretoria. The Dynamic-Q is a multidimensional and robust gradient-based optimisation algorithm that does not require an explicit line search of the objective functions. The technique involves the application of a dynamic trajectory LFOPC optimisation algorithm to successive approximate quadratic sub-problem of the original problem [207], hence the name "DYNAMIC-Q". The DYNAMIC-Q can handle numerical analyses obtained from CFD and FEM simulations efficiently by dealing with all noise functions due to grid changes, convergence and the numerical accuracy of the computer.

In this method, the successive sub-problems $P[l]$, $l = 0, 1, 2,...$ are generated at successive design points $\mathbf{x}^l$, starting with an initial arbitrary design x^0 to a solution x^*. They develop the spherical quadratic approximations to approximate the objective functions or constraints, or both of the objective functions and constraints, provided that they are not analytically given or very numerically expensive to compute [208,210]. The spherical quadratic approximations are given by:

$$\tilde{f}(x) = f\left(x^{(l)}\right) + \nabla^T f\left(x^{(l)}\right)\left(x - x^{(l)}\right) + \frac{1}{2}\left(x - x^{(l)}\right)^T A\left(x - x^{(l)}\right) \tag{4.7}$$

$$\tilde{g}_i(x) = g_i\left(x^{(l)}\right) + \nabla^T g_i\left(x^{(l)}\right)\left(x - x^{(l)}\right) + \frac{1}{2}\left(x - x^{(l)}\right)^T B_i^{(l)}\left(x - x^{(l)}\right), \quad i = 1,....p \tag{4.8}$$

$$\tilde{h}_j(x) = h_j\left(x^{(l)}\right) + \nabla^T h_j\left(x^{(l)}\right)\left(x - x^{(l)}\right) + \frac{1}{2}\left(x - x^{(l)}\right)^T C_j^{(l)}\left(x - x^{(l)}\right), \quad j = 1,....q \tag{4.9}$$

where $\nabla^T f$, $\nabla^T g_i$ and $\nabla^T h_j$ denote the gradient vector, and can be approximated by a forward finite-difference scheme if these vectors are not known analytically. A, $B_i^{(l)}$ and $C_j^{(l)}$ are approximate Hessian matrices of the objective function, inequality constraint and equality constraint functions respectively. The approximations are defined by the diagonal matrix as

$$A = diag\left(a, a, ..., a\right) = aI \tag{4.10}$$

$$B_i = b_i I \tag{4.11}$$

$$C_j = c_j I \tag{4.12}$$

where **I** represents the identity matrix.

The convergence of the solution is achieved in a stable manner and controlled by imposing move limits on the design variables during the optimisation process. The move limit δ_l takes on the form of the constraint by limiting the movement of each

design variables x_l^k and not allowing the new design point to move too far away from the current design point. The move limit of single inequality constraints is described as

$$g_\delta\left(x_i\right)\left\|x_i - x_i^{l-1}\right\|^2 - \delta_i^2 \leq 0, \quad i = 1, 2, \dots n \tag{4.13}$$

where δ_i is the approximately chosen step limit for each design variable.

The Dynamic-Q is terminated when either the normalised step size is:

$$\Delta x_{norm} = \frac{\left\|x_i - x_i^{l-1}\right\|}{1 + \left\|x_i\right\|} \leq \varepsilon_x \tag{4.14}$$

or the normalised change in the function value is:

$$\Delta f_{norm} = \frac{\left|f_i - f_{best}\right|}{1 + \left|f_{best}\right|} \leq \varepsilon_f \tag{4.15}$$

where ε_x and ε_f are the step size and function value tolerances respectively.

4.5. FORWARD DIFFERENCING SCHEME FOR GRADIENT

APPROXIMATION

The gradient vector of the objective function (obtained from the numerical simulation) at a specified design point x with respect to each of the design variables x_i is approximated by the first- order forward differencing scheme given as

$$\frac{\partial f(x)}{\partial x_i} \approx \frac{f\left(x + \Delta x_i\right) - f(x)}{\Delta x_i} \quad i = 1, 2...., n \tag{4.16}$$

where $\Delta x_i = \left[0, 0, ..., \Delta x_i, ...0\right]^T$, is the suitable step size.

The inequality and equality constraints gradient vectors on the other hand are also approximated within the algorithm by the first- order forward differencing scheme in a similar way. They are represented (4.17) and (4.18) respectively as:

$$\frac{\partial g_j(x)}{\partial x_i} \approx \frac{g_j\left(x + \Delta x_i\right) - g_j(x)}{\Delta x_i} \quad j = 1, 2...., p \tag{4.17}$$

$$\frac{\partial h_k(x)}{\partial x_i} \approx \frac{h_k\left(x + \Delta x_i\right) - h_k(x)}{\Delta x_i} \quad k = 1, 2...., q \tag{4.18}$$

4.6. EFFECT OF THE NOISY FUNCTIONS OF THE FORWARD DIFFERENCING SCHEME ON THE OPTIMISATION ALGORITHM

Noisy functions could occur in objective functions in many engineering design problems. They comprise experimental and numerical simulation analyses as a result of the activities of a complex sequence of calculations involving measured or computed quantities. This may lead to inaccurate solutions. Experimental noise may cause error due to the influence of the environment, while numerical noise may be caused by changes of grid, convergence problems during iterations and numerical accuracy of the computer. The size of the step Δx used in the differencing scheme is very important when approximating the derivative functions. If the size of the step is not carefully chosen, it can pose a noise that result in incorrect solutions [211 - 215]. Therefore, it is essential to choose a step size Δx carefully so that it drastically minimises the noise and gives an accurate representation of the global gradient of the function.

Figure 4.2 shows the effect of noise on the selection of the step size Δx of a function obtained from a numerical simulation. Ideally, a very small step size Δx is expected to give an accurate approximation of the global gradient of a function. However, due to the existence of noise function in optimisation algorithms, the approximation of the global gradient of the function may be inaccurate when a small step size Δx is used as shown in Figure 4.2(a). Thus, using a large enough step size will reduce the

influence of the noise as shown in Figure 4.2(b), but this will also lead to a wrong or inaccurate approximation of the gradients.

To ensure that the step size chosen is ideal, the optimisation problem should be worked out several times with different starting guesses. If the solution converges to the same value, then it can be concluded that the step size is sufficient. If discrepancies are observed, however, the step size should be modified until discrepancies in the results are extremely reduced.
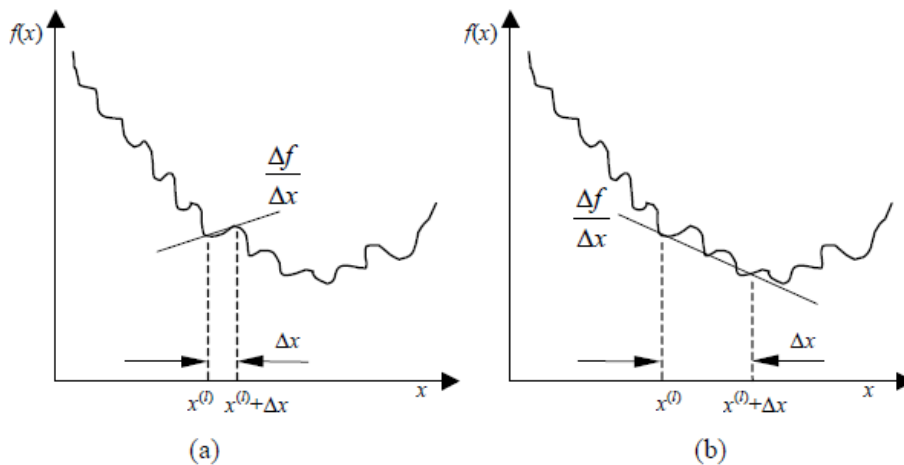

Figure 4. 2 ： Graph depicting the effect of step size on gradient approximation [192]

4.7.   CONCLUSION

This chapter focused in details on the mathematical optimisation algorithms used in this study, namely the LFOPC and DYNAMIC-Q algorithms. The DYNAMIC-Q, which builds on the LFOPC algorithm, presented a multi-dimensional, accurate,

reliable and robust penalty method for solving practical constrained engineering design problems and helps in the optimal design of systems. The effect of numerical noise function during simulation and its effect on the gradient-based optimisation algorithms were also discussed and an efficient way of dealing with the associated problems was suggested.

5

CHAPTER 5: INTERSECTION OF ASYMPTOTES METHOD FOR CONJUGATE CHANNELS WITH INTERNAL HEAT GENERATION[1],[2]

5.1. INTRODUCTION

This chapter deals with the theoretical analysis of geometrical optimisation. It is presented for different configurations using the intersection of asymptotes method to provide the existence of an optimal geometry that minimises the global thermal resistance.

---

[1] This research chapter, together with Chapter 6, has been published in part: O.T. Olakoyejo, T. Bello-Ochende and J.P Meyer, "Constructal conjugate cooling channels with internal heat generation", *International Journal of Heat and Mass Transfer*. Vol. 55, pp. 4385 - 4396, 2012.

[2] This research chapter, together with Chapter 6, has been published in part: J.P Meyer; O.T. Olakoyejo and T. Bello-Ochende, "Constructal optimisation of conjugate triangular cooling channels with internal heat generation", *International communication of Heat and Mass Transfer*, Vol. 39, pp. 1093 - 1100, 2012.

5.2. OVERVIEW OF THE INTERSECTION OF ASYMPTOTES METHOD

This section presents and develops a theoretical solution to the optimal channel geometry of parallel channels with different cross-sectional shapes that penetrate and cool a volume with uniformly distributed internal heat generation, q_s'''.

The cooling fluid is water which is assumed to be in single-phase, steady and a Newtonian fluid with constant thermo-physical properties. The flow is laminar and is forced through the cooling channels by a specified pressure difference ΔP, across the axial length of the structure. Water is more effective than air because the air-cooling techniques are not likely to meet the challenge of high heat dissipation in electronic packages [216, 217].

The total volume and the volume porosity (ϕ) occupied by the channels are fixed. The objective is to achieve minimum global thermal resistance.

In this study, five different types of channel configurations namely cylindrical, square, equilateral and isosceles right triangular and rectangular channels are introduced as shown in Figure 5.1.
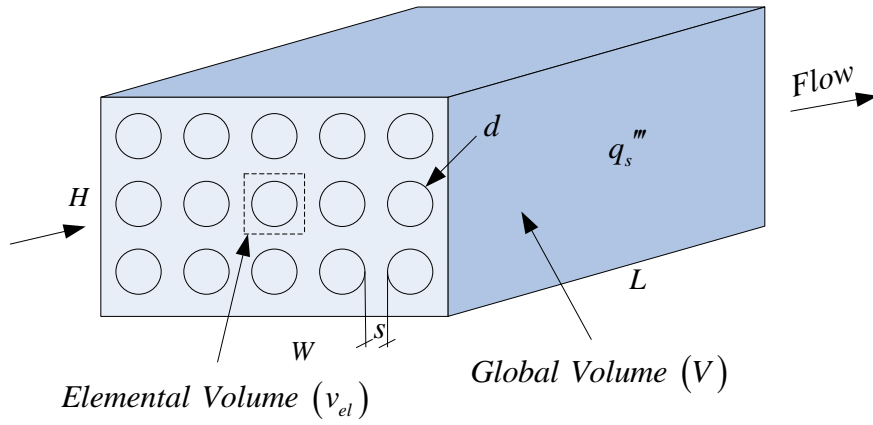
(a)
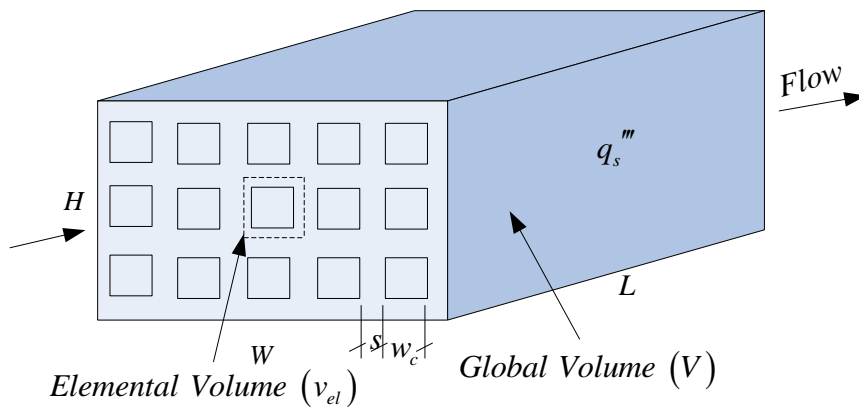
(b)
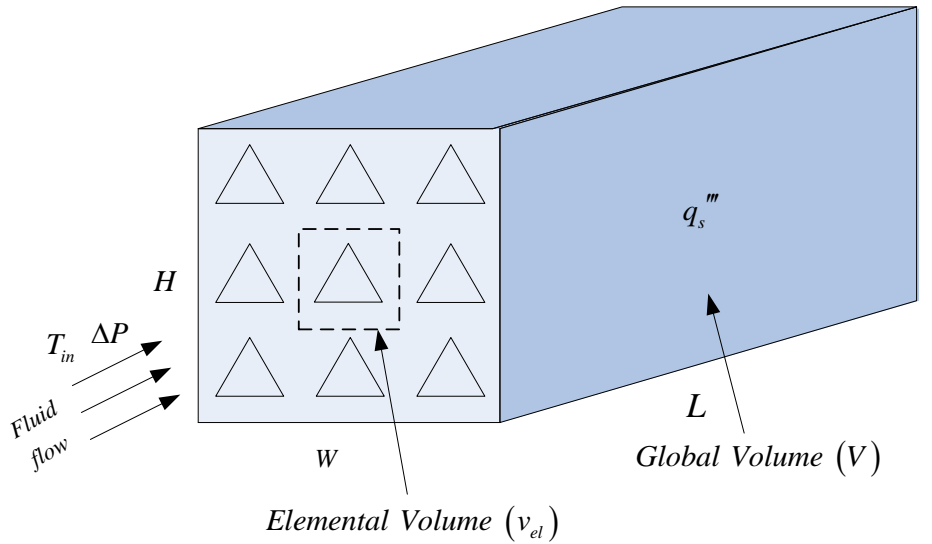
(c)
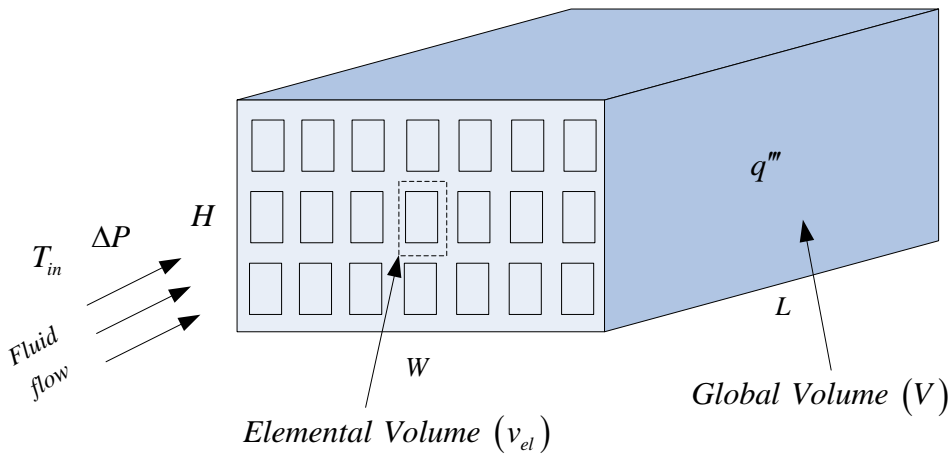
(d)

Figure 5. 1 : Ducts with (a) cylindrical (b) square (c) triangular (d) rectangular cooling channels

The optimisation is based on the intersection of asymptotes method and scale analysis. The optimal channel geometries and minimum global thermal resistance between volume and coolant are reported for all the configurations. The optimal

geometries are determined as trade-offs between the two operating extremes of each configuration channel in which the heat transfer mechanism operates – the extreme limit of a small channel with fully developed flow and the extreme limit of a large channel with the distinct boundary layer.

The following assumptions are also made throughout the analysis: the inlet temperature and the pressure difference ΔP are fixed with a uniform flow distribution in all the channels, laminar flow, constant cross-sectional area of the channels, negligible inlet and exit plenum losses, and negligible axial conduction. An elemental volume is considered because of the symmetry of the heat distribution.

The heat generated in the elemental volume [17, 19] is

$$\dot{q} = q''' \left(A_s - A_c \right) L \tag{5.1}$$

The heat is conducted and deposited as the heat flux, q'', through the solid wall to the fluid, therefore,

$$q''' \left(A_s - A_c \right) L = q'' P_c L \tag{5.2}$$

The porosity is assumed to be fixed at $\phi = A_c / A_s$, therefore Equation (5.2) becomes

$$q'' = \frac{1}{4} q''' d_h \beta \tag{5.3}$$

where β is the numerical value determined from the porosity of the channel and is defined as:

$$\beta = \left(\frac{1-\phi}{\phi} \right) \tag{5.4}$$

and d_h is the channel hydraulic diameter defined as:

$$d_h = \frac{4A_c}{P_c} \tag{5.5}$$

The global thermal resistance or global thermal conductance will be determined in two extreme limits.

5.2.1. Extreme limit 1: small channel

When the channel's characteristic dimension is very small and very slender, that is $d_h \rightarrow 0$ and $d_h \square L$, the flow is fully developed along the length, *L*. See Figure 5.2 for its cylindrical configuration
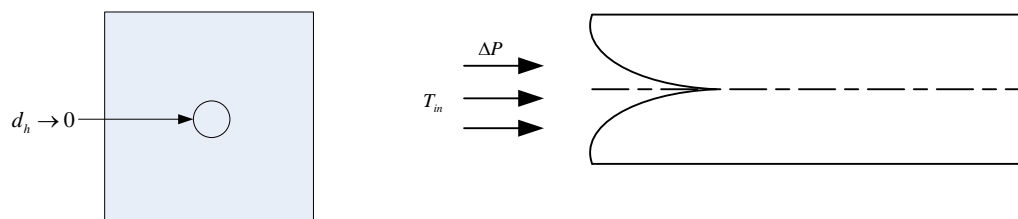
Figure 5. 2 : The extreme limit of the channel's characteristic dimension is very small and very slender, i.e. $d_h \rightarrow 0$ **and** $d_h \square L$

According to the first law of thermodynamics, the rate of heat transfer in a unit volume to the working fluid is equal to enthalpy gained by the working fluid, and then for constant, C_p

$$\dot{q}_s = \rho A_c \bar{u} C_p \left(T_{out} - T_{in} \right) \tag{5.6}$$

In this extreme limit, the fluid in the channel quickly becomes a fully developed flow and the working fluid is overworked in such a way that the outlet temperature T_{out} approaches the peak temperature, T_{max}, at the solid structure.

Therefore, Equation (5.6) becomes

$$\dot{q}_{sm} = \rho A_c \bar{u} C_p \left(T_{max} - T_{in} \right) \tag{5.7}$$

This is equal to the heat deposited as heat flux, q'' through the wall to the fluid.

Therefore,

$$\rho A_c \bar{u} C_p \left(T_{max} - T_{in} \right) = q'' P_c L \tag{5.8}$$

when the flow is fully developed, the average velocity $\bar{u}$, is given by Hagen-Poiseuille as:

$$\bar{u} = \frac{\Delta P \varsigma^2}{4 \mu P_{o_\varsigma} L} \tag{5.9}$$

where ς is the characteristic dimension used to define the Poiseuille number, P_o, and in this case the hydraulic diameter, d_h.

Combine Equations (5.8) and (5.9) and substitute ς for d_h, then rearrange to get

$$\left(T_{\max} - T_{in}\right) = q'' \left(\frac{16 \mu P_{o_{d_h}} L^2}{\rho d_h{}^3 C_p \Delta P}\right) \tag{5.10}$$

Substitute Equation (5.3) for Equation (5.10) and rearrange to get

$$\frac{\left(T_{\max} - T_{in}\right)}{q''' L^2} = \beta \left(\frac{4 \mu P_{o_{d_h}}}{\rho d_h{}^2 C_p \Delta P}\right) \tag{5.11}$$

But

$$C_p = \frac{k_f \Pr}{\rho \nu} \tag{5.12}$$

Substitute Equation (5.12) for Equation (5.11) and rearrange the formula as

$$\frac{k_f \left(T_w - T_{in}\right)}{q''' L^2} = \beta \left(\frac{4 \mu \nu P_{o_{d_h}}}{d_h{}^2 \Pr \Delta P}\right) \tag{5.13}$$

The dimensionless global thermal resistance is defined in terms of dimensionless pressure difference as

$$R = \left[\frac{k_f \left(T_w - T_{in}\right)}{q''' L^2}\right] \cong 4 P_{o_{d_h}} \beta \left(\frac{d_h}{L}\right)^{-2} Be^{-1} \tag{5.14}$$

where

$$Be = \frac{\Delta P L^2}{\mu \alpha} \tag{5.15}$$

From Equation (5.14) for a smaller channel $d_h \, \square \, L$, the thermal resistance is inversely proportional to $d_h{}^2$. Keeping β (which is a function of porosity) constant, it shows that the global thermal resistance increases as the hydraulic diameter decreases.

5.2.2. Extreme limit 2: large channel

In this extreme limit, the channel's characteristic dimension is sufficiently large, that is, $d_h \to \infty$, the boundary layer of surface becomes distinct and the channel diameter is larger than the boundary layer thickness. The working fluid is not properly utilised and working fluid outside the boundary layers becomes useless and the body is not properly cooled in the downstream for cylindrical configuration (Figure 5.3).
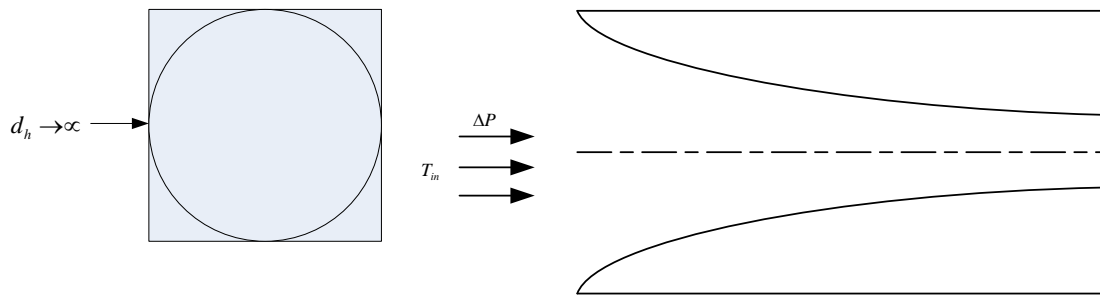
Figure 5. 3 : The extreme limit of the channel's characteristic dimension is sufficiently large, that is $d_h \to \infty$

The rate of heat transfer across the thermal boundary layer is

$$\dot{q}_l = hA_s \left(T_{\max} - T_{in} \right) \tag{5.16}$$

and the heat flux is

$$\dot{q}_l'' = h\left(T_{\max} - T_{in}\right) \tag{5.17}$$

The heat transfer rate can be related to the Nusselt number and heat transfer coefficient over the unit system. The heat transfer coefficient is defined for a laminar boundary layer as [31]

$$\frac{hL}{k_f} = 0.453 k_f \, \mathrm{Pr}^{1/3} \, \mathrm{Re}^{1/2}, \qquad \text{for,} \quad 0.5 < \mathrm{Pr} < 10 \tag{5.18}$$

Substitute Equation (5.18) for (5.17) to get

$$\dot{q}_l'' = \frac{0.453 k_f \, \mathrm{Pr}^{1/3} \, \mathrm{Re}^{1/2}}{L}\left(T_{\max} - T_{in}\right) \tag{5.19}$$

where

$$\mathrm{Re}_L = \frac{\bar{u}_\infty L}{\nu} \tag{5.20}$$

and u_∞ is the free-stream velocity that sweeps the boundary layers. The longitudinal pressure force balance on the control volume inscribed inside a unit volume channel is:

$$\Delta P A_c = P_c L \bar{\tau}_w \tag{5.21}$$

where $\bar{\tau}_w$ is the average wall shear stress across the length and can be obtained from the laminar boundary layer flow solution [218] as

$$\bar{\tau}_w = 0.664 \rho u_\infty^2 \, \mathrm{Re}_L^{-1/2} \tag{5.22}$$

Combine Equations (5.5) and (5.20) with Equation (5.22) to obtain

$$\text{Re}_L = \left(\frac{\Delta P d_h L}{2.656 \rho v^2} \right)^{2/3} \tag{5.23}$$

Substitute Equation (5.23) for Equation (5.19) to obtain

$$\dot{q}_l'' = \frac{0.3271 k_f \, \text{Pr}^{1/3}}{L} \left(\frac{\Delta P d_h L}{\rho v^2} \right)^{1/3} \left(T_{\max} - T_{in} \right) \tag{5.24}$$

Further substitution of Equation (5.3) for Equation (5.24) and rearrangement of the formula defines the dimensionless global thermal resistance as:

$$R = \left[\frac{k_f \left(T_{\max} - T_{in} \right)}{q''' L^2} \right] \cong 0.7643 \beta \left(\frac{d_h}{L} \right)^{2/3} Be^{-1/3} \tag{5.25}$$

From Equation (5.25), for a larger channel, the global thermal resistance is directly proportional to $d_h^{2/3}$. Keeping β (which is a function of porosity) constant, confirms that as the hydraulic diameter becomes larger, the global thermal resistance increases.

5.2.3. Optimal channel diameter and spacing

The optimal behaviour of asymptotes is shown in Figure 5.4 where the fluid is fully developed and utilised. The geometric optimisation in terms of channel could be achieved by combining Equations (5.14) and (5.25), and using the intersection of asymptotes method as shown in Figure 5.5.
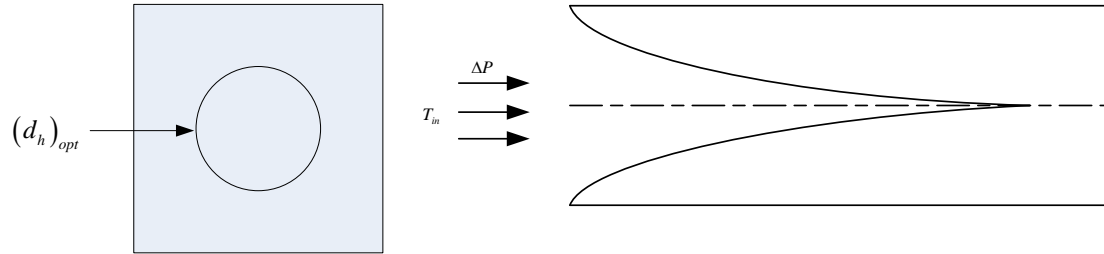
Figure 5. 4 : The optimal limit of the channel's characteristic dimension

The optimal dimension can generally be approximated for the two configurations as the hydraulic diameter where the two extreme curves intersect. The intersection result is

$$\left(\frac{d_h}{L}\right)_{opt} \approx 1.8602 P_{o_{d_h}}^{3/8} Be^{-1/4} \tag{5.26}$$

where $d_{h_{opt}}$ is the optimal hydraulic diameter and for circular channel $P_{o_{d_h}} = 8$. Hence Equation (5.26) reduces to

$$\left(\frac{d_h}{L}\right)_{opt} \approx 4.057 Be^{-1/4} \tag{5.27}$$
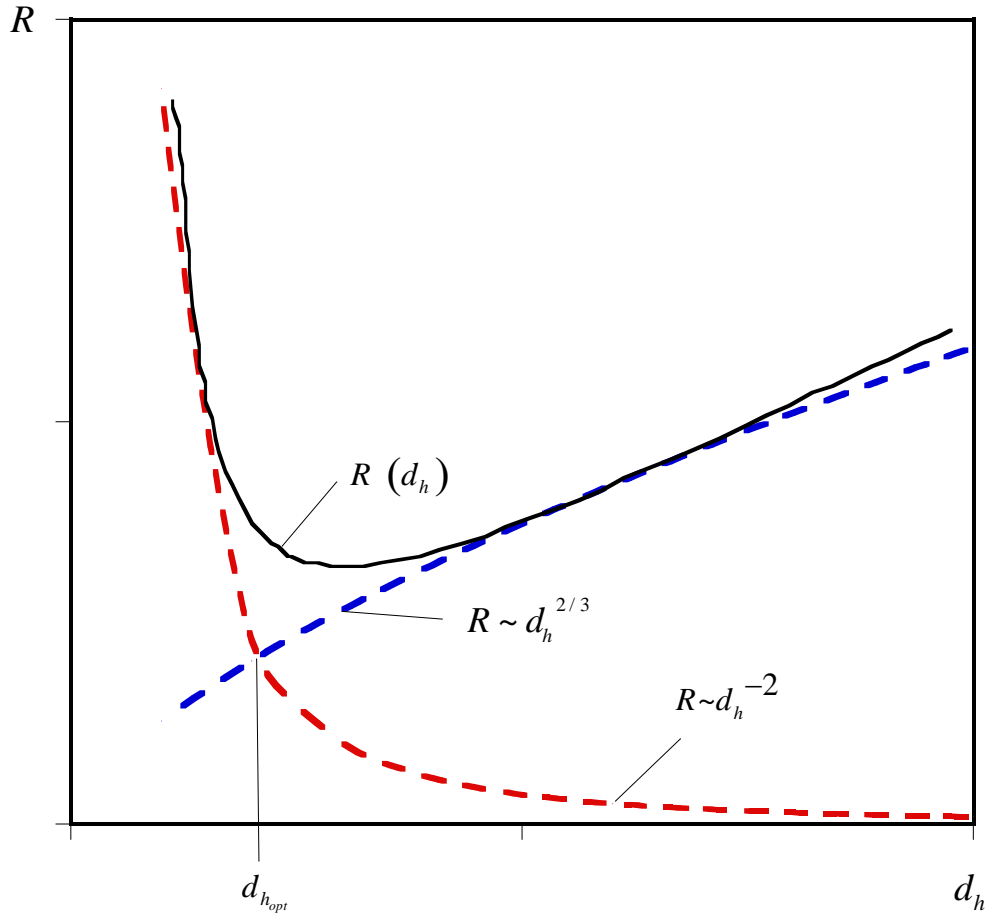
Figure 5. 5 : Intersection of asymptotes method: Global thermal resistance

For a square channel with hydraulic diameter d_h, $P_{o_{d_h}} = 7$

Hence Equation (5.26) reduces to:

$$\left(\frac{d_h}{L}\right)_{opt} \approx 3.859 Be^{-1/4} \tag{5.28}$$

for an isosceles right triangle channel with hydraulic diameter d_h, $P_{o_{d_h}} = 6.577$,

Equation (5.26) therefore reduces to

$$\left(\frac{d_h}{L}\right)_{opt} \approx 3.7698 Be^{-1/4} \tag{5.29}$$

For an equilateral triangle channel with hydraulic diameter d_h, $P_{o_{d_h}} = 6.625$ Hence

Equation (5.26) reduces to:

$$\left(\frac{d_h}{L}\right)_{opt} \approx 3.7801 Be^{-1/4} \tag{5.30}$$

For a rectangular channel, the Poiseuille number can be approximated as

$$P_{o_{d_h}} = \frac{12}{\left(1 + AR_c^{-1}\right)^2 \left[1 - \frac{192}{\pi^5} AR_c^{-1} \tanh\left(\frac{\pi}{2} AR_c\right)\right]} \tag{5.31}$$

hence Equation (5.26)   combined with Equation (5.30)   can be rewritten followed as:

$$\left(\frac{d_h}{L}\right)_{opt} \approx 4.7234 \left[\left(1 + AR_c^{-1}\right)^2 \left[1 - \frac{192}{\pi^5} AR_c^{-1} \tanh\left(\frac{\pi}{2} AR_c\right)\right]\right]^{-3/8} Be^{-1/4} \tag{5.32}$$

The optimal spacing s_{opt} follows from Equations (3), (5) and (5.26):

$$\left(\frac{s}{L}\right)_{opt} \approx 1.8602 \left[\left(1 + \beta\right)^{1/2} - 1\right] P_{o_{d_h}}^{3/8} Be^{-1/4} \tag{5.33}$$

Equations (5.26) and (5.33) show that in the two extremes, the hydraulic diameter and

channel spacing decreases as the pressure difference increases for fixed porosity.

The minimum dimensionless global thermal resistance can be obtained for an

elemental volume for all the channels configurations that correspond to the optimal

geometries. This can be by substituting Equation (5.26) into for Equation (5.14):

$$R_{\min} = 1.156 \beta P_{o_{d_h}}^{1/4} Be^{-1/2} \tag{5.34}$$

Equation (5.34) shows that the thermal resistance decreases monotonically as Be increases for a fixed porosity.

The minimised dimensionless global thermal resistance of a circular channel with $P_{o_{d_h}} = 8$ is

$$R_{\min} = 1.9442 \beta Be^{-1/2} \tag{5.35}$$

and the minimised dimensionless global thermal resistance of a square channel with $P_{o_{d_h}} = 7$ is:

$$R_{\min} = 1.8803 \beta Be^{-1/2} \tag{5.36}$$

The minimised dimensionless global thermal resistance of a isosceles right triangle channel with $P_{o_{d_h}} = 6.577$ is

$$R_{\min} = 1.8513 \beta Be^{-1/2} \tag{5.37}$$

and the minimised dimensionless global thermal resistance of a an equilateral triangular channel with $P_{o_{d_h}} = 6.625$ is

$$R_{\min} = 1.8546 \beta Be^{-1/2} \tag{5.38}$$

The minimised dimensionless global thermal resistance of a rectangular channel with approximated $P_{o_{d_h}}$ of Equation. (5.31) is

$$R_{\min} = 2.1516\left[\left(1+AR_c^{-1}\right)^2\left[1-\frac{192}{\pi^5}AR_c^{-1}\tanh\left(\frac{\pi}{2}AR_c\right)\right]\right]^{-1/4}\beta Be^{-1/2} \tag{5.39}$$

5.3. SUMMARY OF THE THEORETICAL OPTIMISATION FOR ALL THE COOLING CHANNEL SHAPES

5.3.1. Effect of Applied dimensionless pressure difference on the minimised dimensionless global thermal resistance

Figure 5.6 shows the minimised dimensionless global thermal resistance as a function of dimensionless pressure difference at optimised design variables for the cylindrical, square, equilateral and isosceles triangular configurations. Minimised thermal resistance monotonically decreases as the applied dimensionless pressure difference number across the axial length increases for fixed porosity. The cylindrical channel has the highest thermal resistance while the triangular channels have the lowest thermal resistance for a given applied dimensionless pressure difference number. This is due to the fact that triangular configurations have high shear stress corners. Also, Figure 5.7 shows the minimised dimensionless global thermal resistance as a function of dimensionless pressure difference at optimised design variables for rectangular configurations. Minimised thermal resistance decreases as the applied dimensionless pressure difference number across the axial length at different aspect ratios increases.
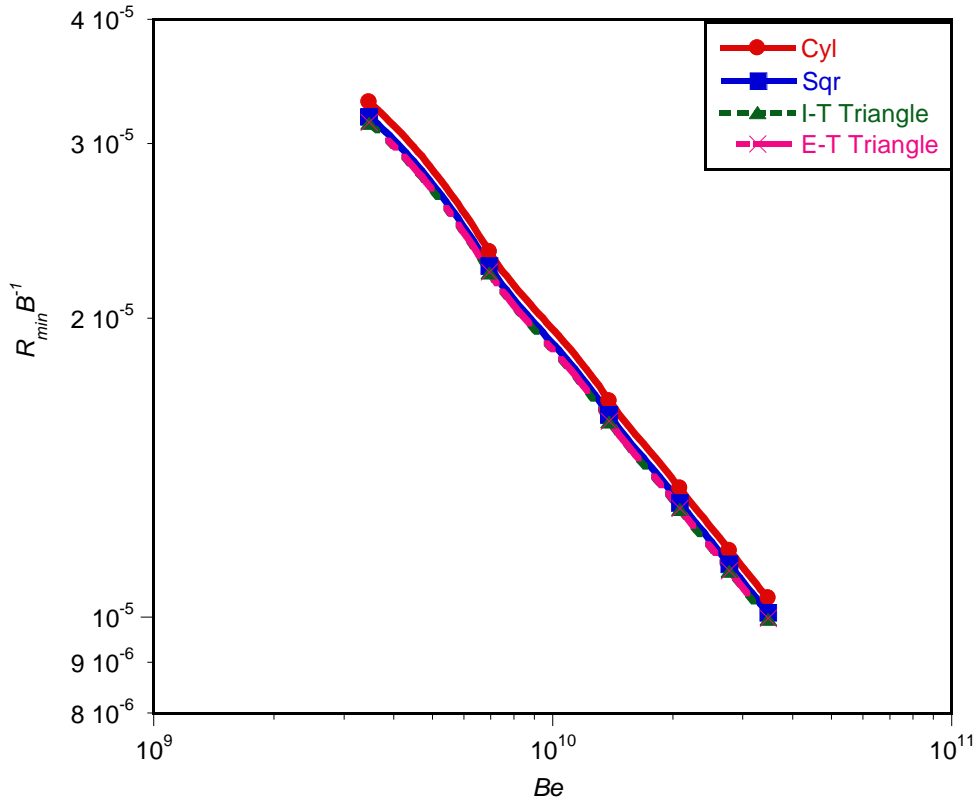
Figure 5. 6 : Effect of applied dimensionless pressure difference on the dimensionless global thermal resistance

5.3.2. Effect of applied dimensionless pressure difference on optimised design variables

Figure 5.8 shows the effect of the dimensionless pressure difference on the optimised hydraulic diameter for the cylindrical, square, equilateral and isosceles triangular configurations. The curve shows that design variables decrease as the applied dimensionless pressure difference for fixed porosity increases. The graph also shows

71

that unique optimal design geometries exist for each applied dimensionless pressure number and for each configuration.

Furthermore, Figure 5.9 shows the graph of dimensionless pressure difference as a function of the dimensionless hydraulic diameter for the rectangular configuration. The curve indicates that optimised the dimensionless hydraulic diameter decreases as the applied dimensionless pressure difference for fixed porosity increases. The graph also shows that unique optimal design geometries exist for each applied dimensionless pressure difference at different aspect ratios.
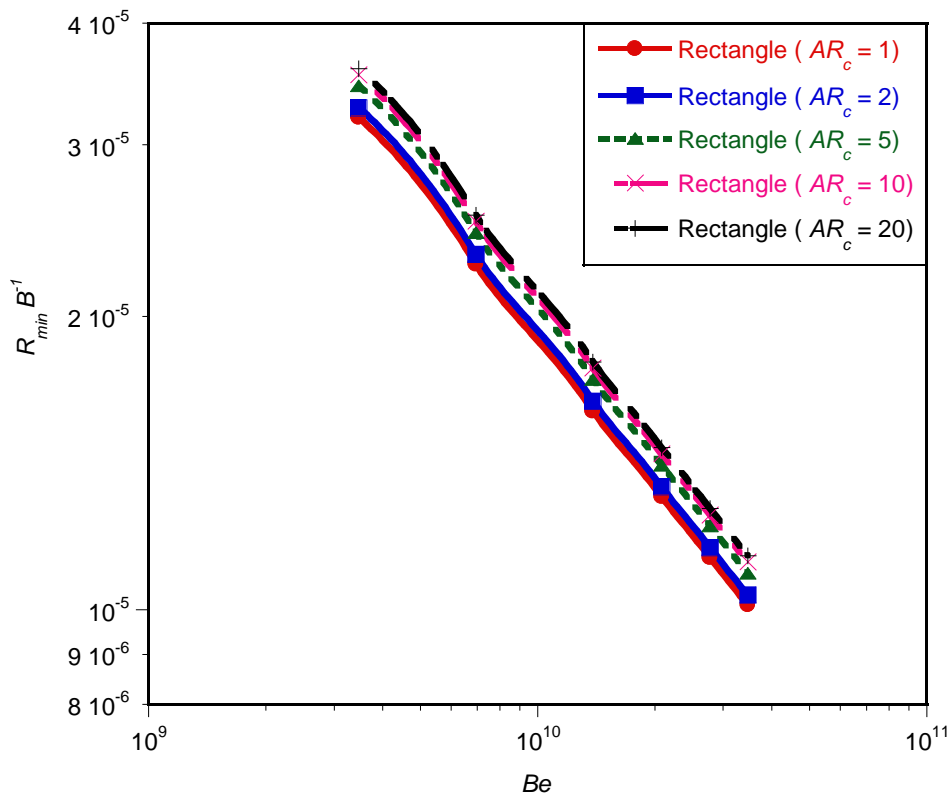

Figure 5. 7 : Effect of applied dimensionless pressure difference on the dimensionless global thermal resistance

In summary, the best parallel-channel structure for suppressing the hot spots of heat-generating devices should have the hydraulic diameter shown in Equation (5.26). The minimised global thermal resistance decreases further by increasing the applied pressure difference number (*Be*) and reducing the channel-to-channel spacing and hydraulic diameter smaller.
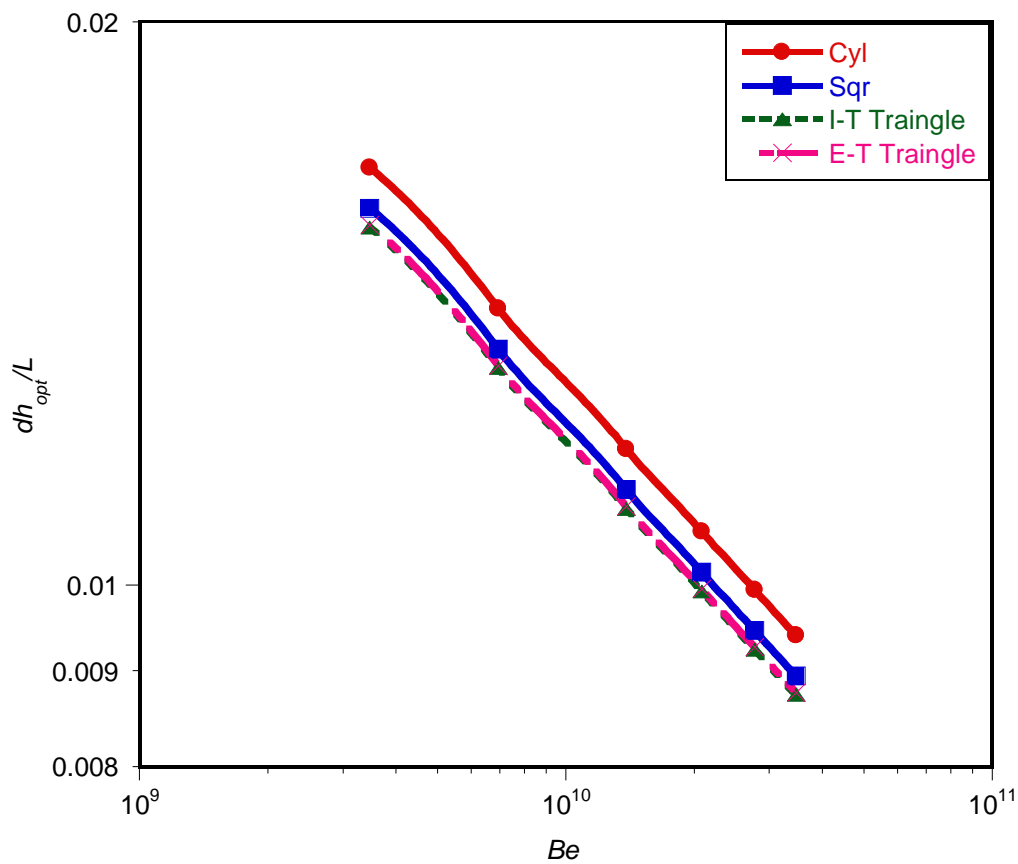
Figure 5. 8 : Effect of applied dimensionless pressure difference on the dimensionless global thermal resistance
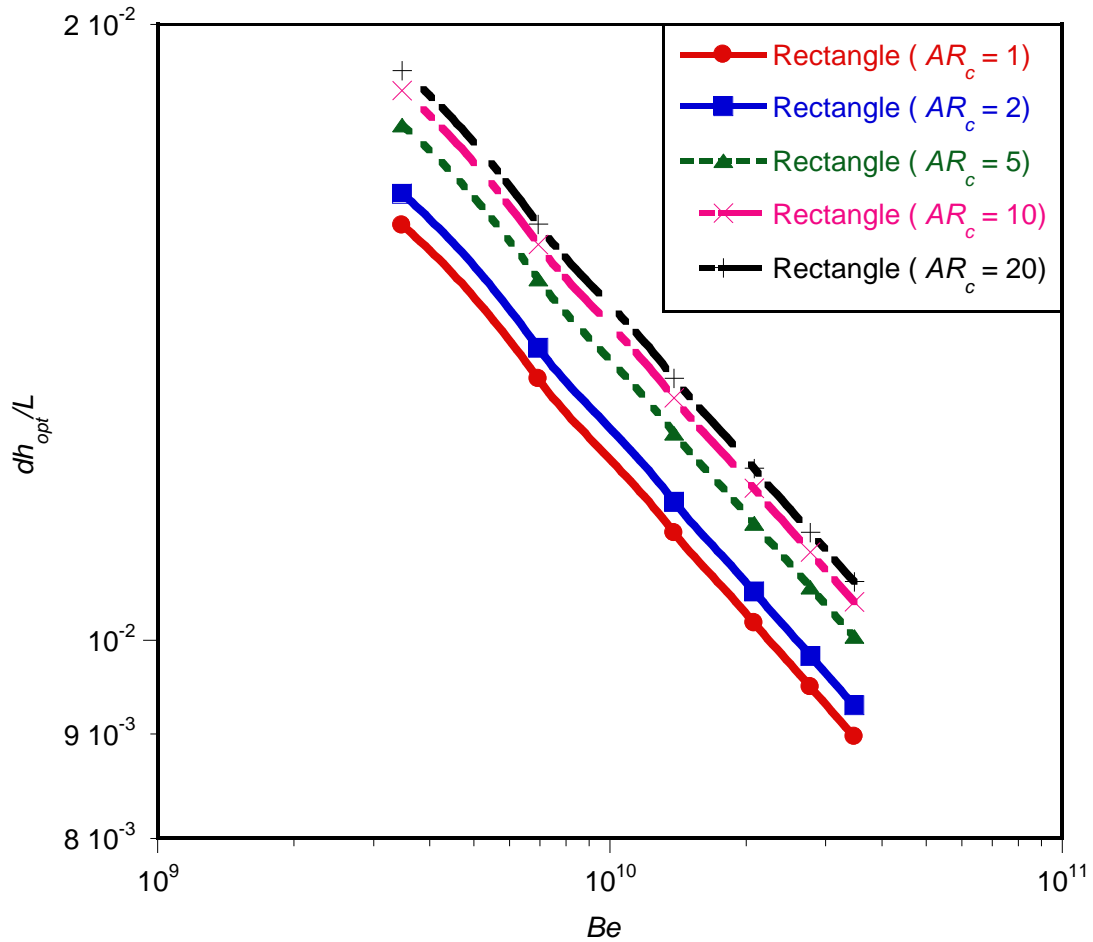
Figure 5. 9 : Effect of applied dimensionless pressure difference on the dimensionless global thermal resistance

5.4. CONCLUSION

This chapter presented and developed an overview of the analytical solution to the geometrical optimisation of the external structures and internal architectures of parallel channels of different cross-sectional shapes for cooling volumes that generate heat uniformly. The intersection of asymptotes method was used to provide the existence of an optimal geometry, which minimises the global thermal resistance.

74

The cooling fluid is driven by forced convection through the channels by the pressure difference across the channels. The optimal channel geometry was determined as a trade-off between the two extremes in which the heat transfer mechanism operates, in other words the extreme limit of the small channel and extreme limit of the large channel. The porosity of the volume penetrated by the array of channels was assumed given.

The optimal spacing between adjacent channels in the array can be derived from the optimal channel sizes already determined. The structure of channels and channel-to-channel spacing are optimal when each flow passage is just long enough to allow for its thermal boundary layers to merge at the exit as shown in Figure 5.4. This can be done by ensuring that the cooling volume is used to its fullest by packing the channels in such a way that every portion of flow passage is worked in a heat transfer form.

The next chapter will provide the numerical solutions for achieving optimal geometry, which minimises the global thermal resistance. The theoretical and the numerical solutions will also be compared.